Int. J. Radiation Oncology Biol. Phys., Vol. 48, No. 2, pp. 571–582, 2000

0360-3016/00/$–see front matter

ELSEVIER

PII S0360-3016(00)00686-6

BIOLOGY CONTRIBUTION

SPATIAL RELATIONSHIP BETWEEN HYPOXIA AND THE (PERFUSED) VASCULAR NETWORK IN A HUMAN GLIOMA XENOGRAFT: A QUANTITATIVE MULTI-PARAMETER ANALYSIS

PAUL F. J. W. RIJKEN, M.SC.,* HANS J. J. A. BERNSEN, PH.D.,† JOHANNES P. W. PETERS,* RICHARD J. HODGKISS, PH.D.,‡ JAMES A. RALEIGH, PH.D.,§ AND ALBERT J. VAN DER KOGEL, PH.D.*

*Department of Radiotherapy, University of Nijmegen, Nijmegen, The Netherlands; †Department of Neurology, Canisius Wilhelmina Hospital, Nijmegen, The Netherlands; ‡Gray Laboratory Cancer Research Trust, Mount Vernon Hospital, Northwood, Middlesex, England; §Radiation Oncology, University of North Carolina School of Medicine, Raleigh, NC

Purpose: To quantitatively study the spatial distribution of tumor hypoxia in relation to the perfused vasculature.
Methods and Materials: Using a human glioma xenograft model, nude mice were administered two different hypoxia markers (NITP or pimonidazole) and the perfusion marker Hoechst 33342. Frozen tumor sections were sequentially scanned for perfusion, hypoxia, and vasculature, respectively, to quantitate perfusion, vasculature, and hypoxia parameters in the same section.
Results: All tumors showed incomplete perfusion. Both NITP and pimonidazole stained the same hypoxic tumor areas. No statistically significant differences between the two markers were observed. The density of the perfused vessels was inversely related to the hypoxic fraction. At critical distances from perfused vessels, hypoxia occurred. These data suggest that predominantly diffusion-limited hypoxia was detected, based on the spatial distribution of nearby vessels. Also, the proportion of hypoxia distributed over arbitrary zones of 50 μm around perfused vessels was calculated. The largest proportion of hypoxia was found at distances beyond 100 μm from perfused vessels.
Conclusion: With the multiple staining and functional microscopic imaging technique described here, the spatial relationship between perfused vessels and hypoxia was quantified in whole tumor cross-sections. The usefulness of this histologically-based method to quantitate morphological and physiological aspects of the tumor microenvironment was evaluated. **© 2000 Elsevier Science Inc.**

Tumor, Perfusion, Vasculature, Hypoxia, Image analysis.

INTRODUCTION

One of the intrinsic factors that determines radiation response of tumors is oxygenation status. Hypoxic tumor cells are more resistant to radiation than well-oxygenated cells (1, 2). It has been demonstrated that hypoxia exists in many experimental tumors (3) and human tumors as well (4–7). Two forms of hypoxia have been identified in tumors. One form is the so-called diffusion-limited or chronic hypoxia, where cells are organized around a blood vessel (8) and have lower pO_2 values at greater distances from the vessel due to oxygen consumption. The other form is based on irregularities in blood flow, causing perfusion-limited or acute hypoxia around blood vessels (9, 10). Both the architecture and functional status of the tumor vascular network will determine the oxygenation in the tumor. Indications for a relationship between the spatial distribution and tumor oxygenation was found by Awwad and coworkers (11); they observed a progressive reduction in the proportion of intercapillary distances greater than 300 μm in cervix carcinoma during the course of pelvis irradiation in patients. Also, theoretical simulations of oxygen delivery to the tissue show that heterogeneity in microvasculature greatly affects the occurrence of hypoxic areas (12). Therefore, it is important to study tumor hypoxia in relation to the functional vascular geometry with direct quantitative measurements of these parameters in the same tumor. Numerous studies have been done to investigate the relationship between tumor perfusion and oxygenation with nuclear medicine assays or MR techniques (13, 14) and histologically (14–20). A sophisticated immunohistochemical method to quantitate the perfused vasculature and hypoxia has been developed by Fenton and coworkers (21). In montage scans from histological sections of KHT tumors, they analyzed the distribu-

Reprint requests to: Paul F. J. W. Rijken, Institute of Radiotherapy, University of Nijmegen, P.O. Box 9101, 6500 HB Nijmegen, The Netherlands. Tel: 24-361-4515; Fax: +31-24-3568350; E-mail: p.rijken@rther.azn.nl

This work was supported by the Dutch Cancer Society and the DHHS (USA) Grant CA50995.

Acknowledgments—We gratefully thank our colleagues from the Central Animal Laboratory for their assistance.

Accepted for publication 8 May 2000.

tion of distances from viable cells to the nearest blood vessel in relation to the binding intensity of the hypoxia marker EF5.

In the present study, we extended a previously developed digital image analysis system measuring the perfused vasculature in montage scans of whole tumor cross-sections (22, 23) for simultaneous detection of hypoxia and the perfused vasculature. This technique has already been shown to be a valuable tool in anti-angiogenesis studies of tumors (24, 25), and also in combined NMR studies (26, 27). A multicolor immunofluorescence-staining technique was applied, using Hoechst 33342 as a perfusion marker and an immunohistochemical marker for anatomical vessels. At this time, three nitroimidazole agents are used worldwide for immunohistochemical detection of cells which are radiobiologically hypoxic: NITP (28), pimonidazole (29), and EF5 (30, 31). The latter two agents can be used in humans (4, 5, 32). Here, we used the first two hypoxia markers: 7-[4′-(2-nitroimidazol-l-yl)-butyl]-theophylline (NITP) (34), and 1-[(2-hydroxy-3-piperidinyl)propyl]-2-nitroimidazole hydrochloride (pimonidazole) (35). The main goal of this study was to obtain a set of two-dimensional morphological and physiological parameters for quantifying the spatial relationship between hypoxia and the perfused vasculature in whole tumor cross-sections.

METHODS AND MATERIALS

Tumors and immunohistochemical staining

A human glioma xenograft (E106), derived from a primary human glioma surgery specimen (glioblastoma multiforme), was used. After successive transplantations of viable tumor tissue subcutaneously in the flank of athymic mice (BALB/c ABom *nu*), eight tumors were studied, with sizes ranging from 147 to 323 mm^3. The experimental procedures were approved by the local ethical committee for animal use.

Four animals were injected i.p. with a 0.3-mL suspension of NITP (Gray Laboratory, Northwood, Middlesex, UK). This suspension consisted of 70 mg NITP in 0.5 mL10% dimethylsulphoxide (DMSO) plus 4.5 mL heated peanut oil. Another four animals were administered 0.05 mL of a solution of 20 mg pimonidazole (Natural Pharmaceuticals, International Inc., Research Triangle Park, NC) in 0.5 mL saline by injection via one of the lateral tail veins.

Two hours after administration of the hypoxia markers, the animals were injected i.v. via one of the lateral tail veins with a 0.05-mL solution of Hoechst 33342 (Sigma Immunochemicals, Zwijndrecht, The Netherlands) in PBS (phosphate buffered saline, pH 7.4) at a dose of 15 mg/kg to determine tumor perfusion. One minute after Hoechst injection, the mice were killed. The tumors were removed quickly, frozen, and stored in liquid nitrogen, which prevented the dye from diffusing too far into the tissue. From each tumor, two frozen sections (5-μm thick; from central areas) were air-dried and fixed in acetone for 10 min, followed by washing with PBS (5 min). After scanning these sections for detection of perfused areas (see next section), slices were further stained to visualize hypoxia and the vasculature. Sections of the NITP-labeled tumors were incubated overnight at 4°C with a 1:10 dilution of rabbit anti-theophylline (Sigma Immunochemicals) in rat anti-mouse-endothelium (Moab-9F1-supernatant, Pathology Department, University Hospital St. Radboud, Nijmegen) solution. 9F1 is a specific mouse endothelial marker (36, 37). Sections of the pimonidazole-labeled tumors were incubated overnight at 4°C with a 1:2,000 dilution of rabbit anti-pimonidazole (38) in rat anti-mouse-endothelium (Moab-9F1-supernatant) solution. For all subsequent steps, all sections were processed equally. After three washes in PBS, the sections were incubated for 60 min at room temperature with a cocktail of donkey anti-rabbit-biotin (Jackson ImmunoResearch Laboratories Inc., West Grove, USA) and goat anti-rat-TRITC (Jackson ImmunoResearch Laboratories Inc.), both diluted 1:100 in PBS with 0.5% BSA-c (Aurion, Wageningen, The Netherlands) and 0.1% Tween-20 (Sigma Immuno Chemicals) for visualizing NITP and the endothelium, respectively. After another triple rinsing, sections were incubated for 60 min at room temperature with a 1:100 dilution of streptavidin-alexa488 (Molecular Probes, Leiden, The Netherlands) in PBS with 0.5% BSA-c (Aurion) and 0.1% Tween-20 (Sigma Immuno Chemicals) for visualizing pimonidazole and the endothelium, respectively. As a final step, sections were washed in PBS and automatically scanned on a fluorescence microscope to detect hypoxia. Following this scan, sections were mounted in fluorstab (Organon, Boxtel, The Netherlands) and covered with a coverslip.

Scanning tumor sections for tumor perfusion, hypoxia, and vasculature

A digital image processing system for analyzing perfusion and vascularity in tumor sections (22) was modified and extended for the analysis of hypoxic regions to study these three parameters simultaneously in the same sections. Fluorescence signals were recorded by a high-resolution intensified solid state video camera (MXRi, HCS, The Netherlands). The video signal was digitized to images with 256-Gy levels. The digital imaging application, TCL-Image (TNO, Delft, The Netherlands), was used for recording and further processing the images and controlling a motorized scanning stage (EK 32, Märzhäuser, Wetzlar, Germany) attached to a fluorescence microscope (Axioskop, Zeiss, 100-Watt short-arc mercury lamp).

Before scanning a series of sections for a particular fluorophore, the automated scanning stage was initialized and calibrated, and a threshold pixel value to segment the objects from the background was determined. For this purpose, an image of a representative region of each stain (Hoechst, 9F1, and NITP or pimonidazole) was recorded and processed to correct for shading effects. Next, the structures of interest were isolated from the background by using an interactive threshold operation available in the analysis package. The threshold value was selected visually

and recorded by the image analysis system and used for automated image thresholding during the subsequent scans of tumor sections. Separate histological sections with binding in the absence of marker administration were evaluated to distinguish the structure of interest from other tissue elements.

The perfused tissue areas stained by Hoechst 33342 were visualized on the fluorescence microscope using a filter with excitation at 365 nm and emission at 420 nm. Preceding the first scan, the starting point was determined by moving the stage with a joystick. The stage coordinates were recorded by the system for later storage. During each scan, which consisted of a selectable meander pattern from 4×4 up to 12×12 fields, the previously recorded threshold value was used to isolate the perfused areas from the background in a binary image. After each scan, a binary composite image with the perfused areas was reconstructed from the recorded and processed binary images of each field (22). Stage coordinates of the starting point were stored within the header of the image file and the latter was saved as a binary image in a bitplane of a grey-value image on the computer.

After immunohistochemical staining for hypoxia, sections were scanned on the image analysis system. A filter combination of 450–490-nm excitation and 520-nm emission was used. Preceding each scan, the corresponding grey-value image with the perfused areas was loaded in computer RAM from the hard disk and the stored stage coordinates were used to move the stage to the starting point automatically. Next, the section was automatically rescanned, and hypoxic regions were detected using the previously determined threshold. All sections of the NITP-labeled tumors were processed in one series. When tumor sections of the pimonidazole-labeled tumors were processed in another series, a new threshold value was determined. As a result of each scan, a binary composite image with all hypoxic regions was reconstructed from the individual recorded and processed images and stored in a different bitplane of the corresponding image with the perfused areas. This new image was saved on the computer.

When all sections had been scanned for hypoxic regions, they were immunohistochemically stained for vasculature and visualized with a 510–560-nm excitation and 590-nm-emission filter. After moving the stage to the starting point, sections were rescanned for detection of vasculature (22). The resulting composite binary image was stored in a new bitplane of the combined image with perfused areas and hypoxic regions and saved on the hard disk for future multiparameter analysis. The tumor area, used as a mask in further analysis, was determined by drawing a line connecting the most outer vascular structures of the tumor, followed by filling the enclosing area. The sequentially recorded composite images of the tumor sections with detected perfused areas, hypoxia and total vascular bed, respectively, were displayed using pseudocolors for each structure; any small shifts between the separate images were corrected manually.

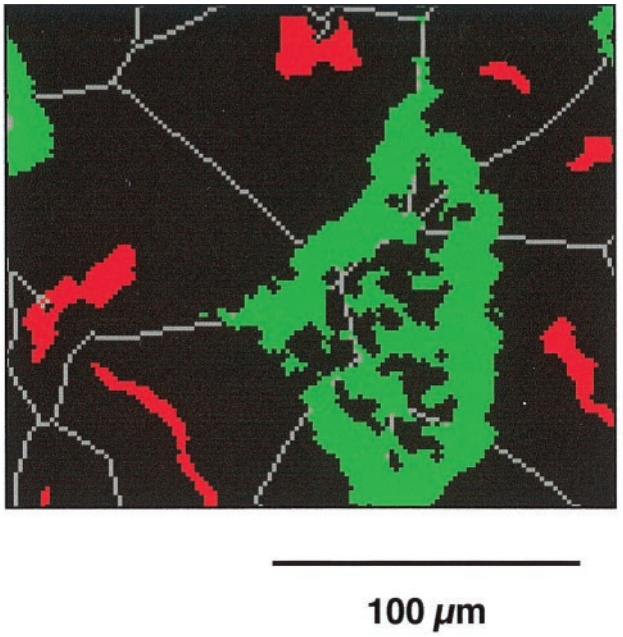

Fig. 1. Detail of a pseudocolored composite digital image reconstructed after repeated scanning of multiple stained sections from human glioma xenografts in nude mice. Minimal distances were calculated (indicated by the white help lines) from perfused vessels (red) to the nearest hypoxic regions (green) in each vascular domain (black), delineated by the dark grey lines.

Multiparameter analysis of vascularity, perfusion, and hypoxia in tumor sections

Vascularity and perfusion. Tumor blood perfusion and vascularity were quantitated as described in a previous paper (22). Briefly, for each tumor section, two composite images with the vascular structures and the perfused areas, respectively, were combined using the logical "AND" operation, resulting in a new image with the overlapping structures representing the Hoechst-perfused vascular structures. The area of the latter structures divided by the total vascular area is the perfused fraction (PF). As a measure of vascularity, the relative vascular area (RVA, the total vascular area divided by the total tumor area), and the number of vascular structures per mm^2 (VD) were calculated. In addition, the perfused vascular density was determined and expressed as the number of perfused vessels per mm^2 (VD_p). The mean values of these parameters of all sections from each tumor were calculated and used in further analysis. Differences between tumor lines were tested using the *t*-test. A significance level of $p = 0.05$ was used.

(Perfused) vasculature and hypoxia. Hypoxia and its relation to the perfused vasculature was quantitated using the digital image analysis system. The hypoxic fraction (HF) was measured in whole tumor sections. Therefore, the ratio of total hypoxic areas (pixels) and the total tumor area (pixels) was calculated from the binary image with the hypoxic regions. In randomly selected regions of interest (ROI), distances from perfused vessels to the nearest hypoxic regions were analyzed (see text below and Fig. 1). ROIs were defined by manually drawing rectangles in a

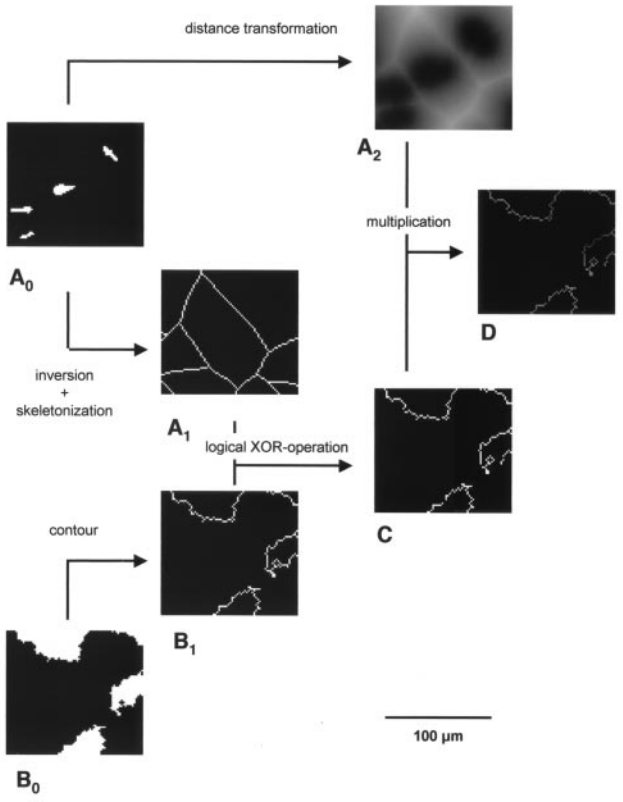

Fig. 2. Schematic illustration of all image processing steps needed to measure distances from perfused vessels to the nearest hypoxic areas in each vascular domain. An image with perfused vessels (A_0) is inverted, followed by skeletonization to determine the boundaries of vascular domains (A_1). Image A_2 is obtained by a distance transform operation of the inverted image A_0: the grey-value of each pixel represents its distance to the edge of the nearest vessel in image A_0. From an image with hypoxia in the same region of interest (B_0), contours of these hypoxic areas were determined (B_1); the latter image and image A_1 were combined, using the binary logical exclusive "OR" operation to define separate contours of hypoxia in each domain (C). Multiplication of image A_2 and image C resulted in an image with contour lines of hypoxic areas of which each pixel represents its distance to the edge of the nearest vessel.

binary image, enclosing regions that contained at least one perfused vessel and a nearby hypoxic region. This binary image was stored as a bitplane in the corresponding grey-value image. HD_{min} was calculated in a number of ROIs per tumor section, varying from 10 to 57, with sizes of 1,027–1580 μm^2.

Minimal distances from perfused vessels to the nearest hypoxic regions (HD_{min}) were analyzed in vascular domains (Fig. 1) by performing several image processing operations (Fig. 2). First, an image with the perfused vessels only (A_0, Fig. 2) was inverted, followed by a skeletonization operation resulting in an image containing lines equidistant to adjacent perfused vascular structures (A_1), representing the boundaries of the vascular domains. Also, from the inverted image with the perfused vessels (A0), a grey-value image with the distance transform was obtained (A_2). Next, from an image with the hypoxic regions in the same ROI (B_0), contours of the hypoxic areas were determined and put into a new image (B_1). This image was processed with the image containing the contours of the vascular domains (A_1) to exclude foreground pixels existing in both images using the binary logical exclusive "OR" operation. The result was an image with the contours of hypoxic regions or parts of it lying in different vascular domains (C). Multiplication of this (binary) image with the distance transform image yielded a grey-value image with contour lines of which each pixel had a value representing the distance to the perfused vascular structure of the domain in which it is lying (D). The minimal pixel value on each line in an image was determined and converted to micrometers and stored into an ASCII-text file. From the frequency distribution of all these values in all sections of a tumor the median minimal hypoxic distance (HD_{min}) was calculated. These values were compared with the spatial distribution of perfused vessels. Therefore, distances between perfused vessels were measured in areas of the tumor with hypoxia ($IVD_{p\text{-}H}$) and without hypoxia ($IVD_{p\text{-}nH}$). This was done by detecting all branchpoints of this skeleton in the image with the outlines of the perfused vascular domains only (image A_2, Fig. 2). The result was stored in another image. A logical exclusive "OR" operation was performed on the resulting image and on the image with the outlines of the domains (A_2) to exclude these branchpoints in the latter image. Next, this image was multiplied with the previously determined distance transform image A_1 (Fig. 2) to obtain a grey-value image with lines containing pixels that had values corresponding to the shortest distance to adjacent perfused vessels. The minimum value for each line was determined, converted to micrometers, and multiplied by 2 to get the distance between the two adjacent vascular structures at that position. Median values for each tumor were calculated from all data of the individual sections.

To quantitate the distribution of hypoxic regions in tumor sections in relation to the perfused vasculature, six arbitrary zones of about 50 μm, 100 μm, 150 μm, 200 μm, 250 μm, and $>$ 250 μm around each perfused blood vessel were defined (Fig. 3). They were generated in binary images from the image with the perfused vessels only, using the binary DILATION operation (7×, 14×, 21×, 28×, and 35×, respectively; resolution is 7.2 μm per pixel) in combination with the logical exclusive "OR" operation.

When an image with all areas of a particular zone was combined with the corresponding image containing the hypoxic regions of the whole section, a new image was generated with the hypoxic areas in only that zone. The sum of all of these hypoxic areas divided by the total hypoxic area in the whole section gave the proportion of hypoxia distributed over this particular zone (HF−distr). This was done for all six different zones.

Adjacent sections of those used for digital analysis of hypoxia, perfusion, and vasculature were stained with hematoxylin and eosin to allow histological examination of necrotic regions. Necrotic areas were excluded manually in

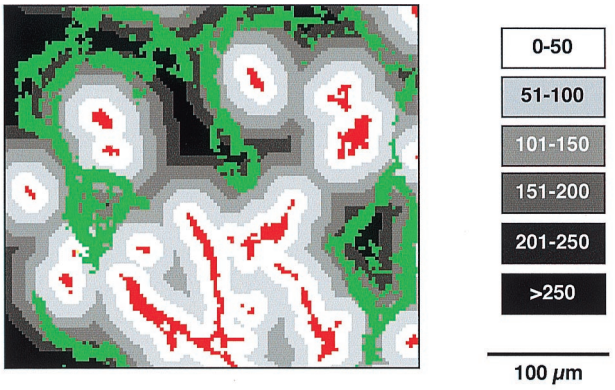

Fig. 3. Detail of a digital image reconstructed after repeated scanning of multiple stained sections from human glioma xenografts in nude mice with the distribution of hypoxic regions in arbitrary zones of 50 μm (grey-values) around perfused vessels (red) determined by the image processing.

the binary image with the detected total tumor area before any automatic analysis started.

To establish the variation in hypoxia measurements between different analysis sessions introduced by the manual threshold settings, one tumor section was scanned and analyzed, without changing the threshold value (grey-value 29) while using the same tumor area as a mask. Next, analyses were repeated using two other grey-values below and above this originally set value (grey-values 25, 27, 31, 33), representing a larger range than the experimental one. This was done for two different tumors.

RESULTS

Immunofluorescence staining

After sequential scanning of tumor sections, perfused and nonperfused tumor vasculature, as well as hypoxia, were detected in the same cross-section with the help of a digital image analysis system described here. All tumors demonstrated hypoxic regions and vascular beds with perfused and nonperfused vessels. The vasculature showing red fluorescence could easily be segmented from the dark background. The perfusion marker Hoechst was restricted to a few cell layers around perfused blood vessels. The intensity of this blue fluorescence signal rapidly decreased with increasing distance from perfused blood vessels. Green immunostaining patterns for NITP and pimonidazole were seen in all tumors and mainly at a distance from (perfused) vessels (Fig. 4). Here, signal intensities were at background levels around (perfused) vessels and increased rapidly to higher values at a certain distance from these vessels; an example of a gradient in one region of interest (ROI) is shown by Fig. 5. The pixel value at the beginning of this steeper gradient (see arrows on Fig. 5) was chosen as the fixed threshold value for isolation of the hypoxia from the background. In this ROI, these values corresponded to different distances between the two hypoxia markers (for NITP at larger distance). If necrosis was present, it was enclosed by a band of hypoxic staining. In a few tumors, staining occurred in the necrotic tissue. During scanning sessions, no changes in threshold settings had to be made by the operator, because of consistent staining results in the entire set of tissue sections examined. The computerized composite images with different histological structures, obtained after sequential scanning a section, highly matched when overlaid. In a few cases, minor manual corrections were needed.

Image analysis of tumor vascularity, perfusion, and hypoxia

The majority of the tumors showed most of the vascular bed being perfused; perfused fractions varied from 0.55 to 0.86. Hypoxic fractions tend to be lower in the NITP-stained tumors compared to the pimonidazole-stained tumors (0.12 ± 0.04 and 0.18 ± 0.09, respectively); however, this difference was not statistically significant.

While no clear correlations were found between perfused fraction and hypoxic fraction, the density of the perfused vessels was inversely related to the hypoxic fraction, which was less obvious when only the NITP-stained tumors were considered (Fig. 6A). In the latter group, the density of all vessels did not show an inverse relationship with the hypoxic fraction of the tumor. Tumor number one, for example, showed both a relatively high hypoxic fraction and vessel density, but not all vessels were perfused (PF = 0.55; Table 1), as is also illustrated by Fig. 4A. However, the pimonidazole-stained tumors did show an inverse relationship (Fig. 6B).

Median values of distances between perfused vessels in nonhypoxic areas varied from 81 to 112 μm in the NITP-stained tumors and from 46 to 121 μm in the pimonidazole-stained tumors. In regions containing hypoxia, median values of distances between perfused vessels were in the range of 158–199 μm in the NITP-stained tumors and 138–199 μm in the pimonidazole-stained tumors. In all tumors, median values of distances between perfused vessels were lower in nonhypoxic regions compared to hypoxic areas (see $IVD_{p\text{-}nH}$ vs. $IVD_{p\text{-}H}$; Fig. 7). In addition, median values of the minimal distances from perfused vessels to the nearest hypoxic cells were almost equal to or lower than the distance between perfused vessels in the corresponding region. Also, the minimal hypoxic distance was almost equal to or higher than the distances between perfused vessels outside hypoxic areas (Fig. 7). Although there was a tendency for lower values of the minimal hypoxic distance in the NITP-stained tumors, no significant differences were found in all three distance parameters between the two tumor groups (Mann-Whitney U-test, $p > 0.39$).

The spatial distribution of all tumor cells stained for hypoxia in relation to the perfused vessels was measured by calculating the proportion of the total hypoxic area in six arbitrary zones around perfused blood vessels. Each zone had a width of 50 μm. The largest proportion of the total hypoxic area, either visualized with NITP or pimonidazole, was found between 100 μm and 200 μm from perfused blood vessels (Fig. 8). Beyond 200 μm from a perfused

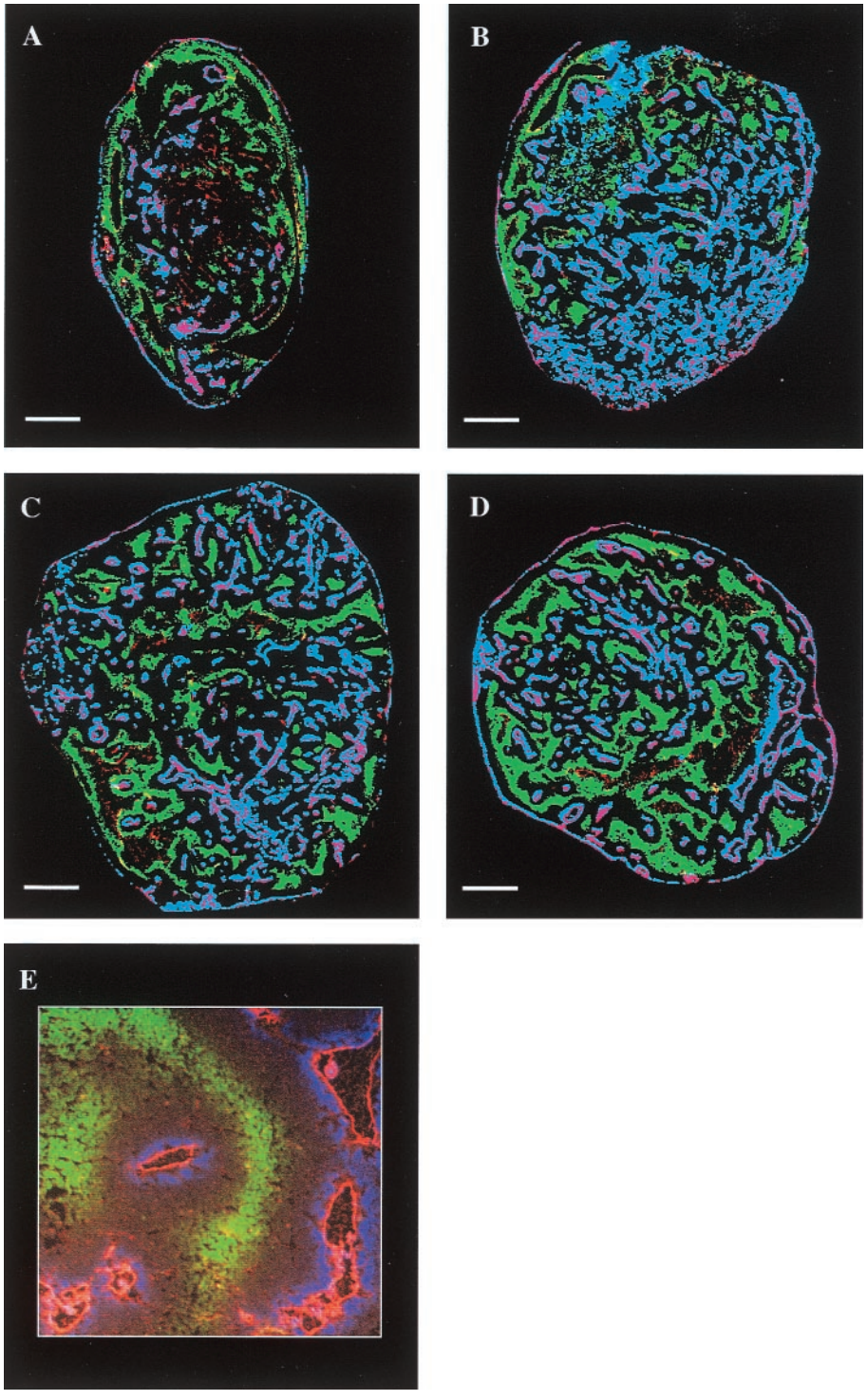

Fig. 4. This figure shows four pseudocolored composite digital images (A, B, C, and D), obtained after sequential scanning for Hoechst perfusion (blue), hypoxia (green), and endothelium (red), respectively, in tumor sections from a human glioma xenograft (E106), and one detailed photograph of a histological section after triple exposure (E). (A) Tumor number 1, with NITP as a hypoxia marker. (B) Tumor number 4 with NITP as a hypoxia marker. (C) Tumor number 6 with pimonidazole as a hypoxia marker. (D) E106 glioma with pimonidazole as a hypoxia marker. Scale bar represents 1 mm. (E) Detail of a fluorescence microscopic image of a E106 glioma; blue is perfusion marker Hoechst, green is pimonidazole, red is an endothelium marker (9F1); magnification is 200×.

vessel, the relative amount of hypoxic area decreased at increasing distance from these perfused vessels. This was due not only to the presence of tumor cells that were dying or necrotic and were not stained by the hypoxia marker for that reason, but also to a decrease of the area occupied by each of the six zones at increasing distance from a perfused

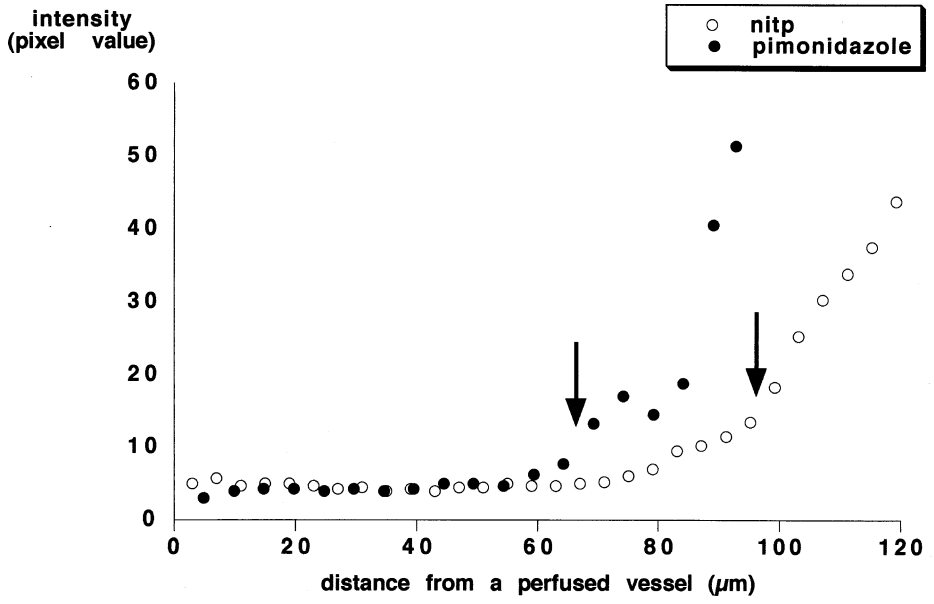

Fig. 5. Hypoxia signal intensities as a function of distance from a perfused vessel in one region of interest is shown. In a grey-value image, recorded in a representative region of an NITP- and pimonidazole-stained section, a line was interactively drawn from perfused vessels to the center of the nearest hypoxic area with maximum binding; on this line, pixel values were determined and plotted against its distance to the perfused vessel. Arrows indicate the chosen fixed threshold for isolation of hypoxic tissue from the lower background.

vessel, as a result of overlap of similar neighboring zones (data not shown).

To study possible variations in threshold settings on the outcome of hypoxia parameters, a section from an NITP-stained tumor and a pimonidazole-stained tumor was analyzed with different threshold values. Threshold values with two- and four-pixel values above and below the originally chosen threshold value in the hypoxia image were taken, while the corresponding images with the perfused areas and vessels, respectively, were kept the same. Hypoxic fractions decreased with increasing threshold values (Table 2). These changes were larger in the NITP-stained tumor (CV = 31.3%) compared to the pimonidazole-stained tumor (CV = 15.5%). The effect of different threshold values on minimal distances from perfused vessels to the nearest hypoxic area was less than on the hypoxic fraction (Table 2). This effect seemed to be larger for the NITP-stained tumor than for the pimonidazole-stained tumor.

The different threshold only influenced the proportion of hypoxia in zones closest to the perfused vessels

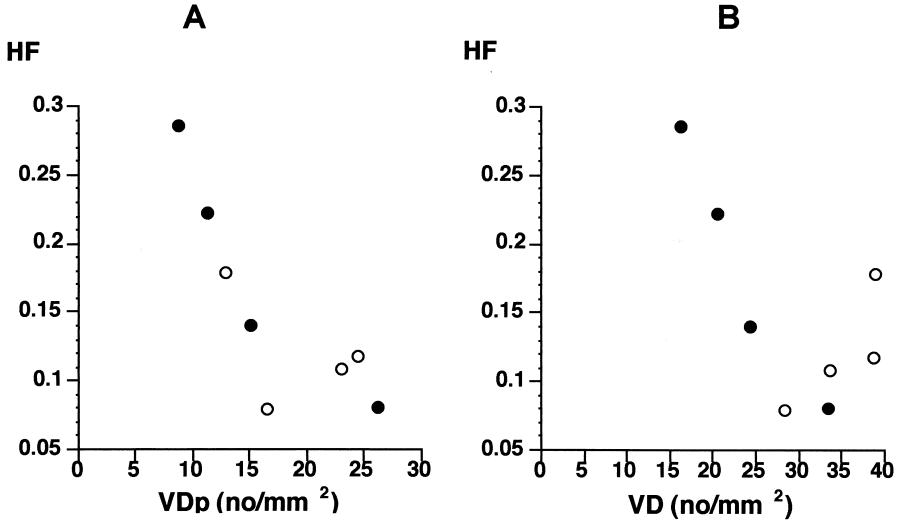

Fig. 6. Relationship between the hypoxic fraction (HF) and the density of perfused vessels (VDp) (A), and density of all vessels (B), respectively, in a human glioma xenograft (E106) after injection of either NITP (open circle) or pimonidazole (closed circle) as the hypoxic marker.

Table 1. Quantitation of blood perfusion, vasculature and hypoxia in a human glioma xenograft (E106) using two different hypoxic markers: NITP or pimonidazole (PIMO)

marker	no*	PF†	RVA‡	VD§	VDp‖	HF¶
NITP	1	0.55	0.073	38.9	12.9	0.18
NITP	2	0.86	0.066	28.3	16.5	0.08
NITP	3	0.86	0.058	33.7	23.0	0.11
NITP	4	0.85	0.073	38.8	24.5	0.12
mean±sd						*0.12 ± 0.04*
PIMO	5	0.49	0.067	16.3	8.7	0.29
PIMO	6	0.75	0.052	24.4	15.1	0.14
PIMO	7	0.82	0.064	20.5	11.3	0.22
PIMO	8	0.80	0.074	33.5	26.2	0.08
mean±sd						*0.18 ± 0.09*
*p***						*0.25*

* = tumor sample number
† = perfused fraction
‡ = the relative vascular area
§ = the vascular density including all vessels
‖ = the vascular density including only perfused vessels
¶ = the fraction of hypoxia relative to total tumor area
** = the Mann-Whitney U test was applied

(Table 3); this effect was largest in the NITP-stained tumor.

DISCUSSION

A multiparameter analysis based on a semi-automatic digital imaging system was developed for quantitation of hypoxia in relation to blood perfusion and vascularity in whole cross-sections of a human glioma xenograft. Detection of multiple fluorescence signals with this sequential scanning technique permitted us to obtain highly matching images from different histological structures in the same specimen.

Although a large degree of heterogeneity in hypoxia and vascularity within tumors and between tumors was observed, and the globally measured perfusion fraction showed no correlation with the hypoxic fraction, the globally measured density of (perfused) vessels was inversely related to the hypoxic fraction. This suggests that the type of hypoxia detected in these gliomas was diffusion-limited and determined by the spatial distribution of perfused vessels. This was also supported by the fact that in highly perfused regions without hypoxia, distances between perfused vessels were smaller than in regions with hypoxic areas surrounding the vessels. As the tumor grows, distances between (perfused) vessels become larger. At some critical distance, hypoxia will develop, depending on the oxygen consumption by the surrounding cells. This minimal hypoxic distance was found to vary between 90–140 μm. These so-called chronically hypoxic areas occur at the lower end of an oxygen concentration gradient from a perfused vessel at distances beyond 100 μm, as was first described by Thomlinson and Gray in 1955 (8). Other studies showed that the size of viable cords in tumors surrounding the

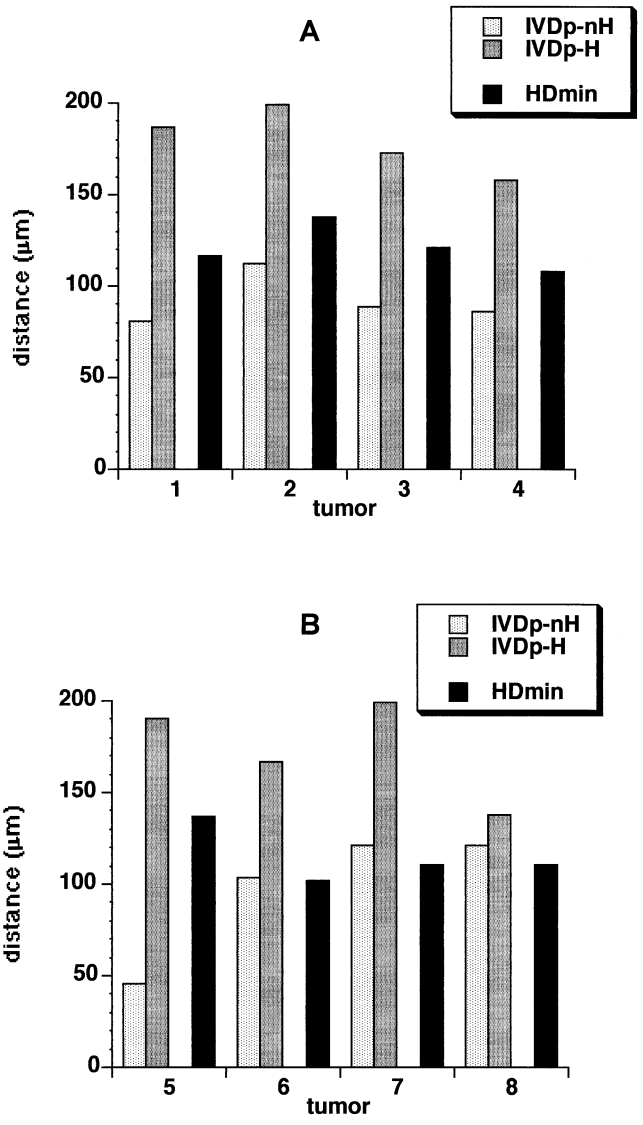

Fig. 7. Distances between perfused vessels with no hypoxia in-between ($IVD_{p\text{-}nH}$) and distances between perfused vessels in hypoxic regions ($IVD_{p\text{-}H}$) were measured in cross-sections of a human glioma xenograft (E106) after injection of either NITP (A) or pimonidazole (B) as the hypoxic marker. In regions of interest of the same sections, minimal distances from perfused vessels to the nearest hypoxic cells (HD_{min}) were calculated. Bars represent median values in microns.

capillaries could vary between 60 and 120 μm (39–41). Beyond a critical point, when distances between (perfused) vessels in hypoxic areas become larger (Fig. 7), more cells will become hypoxic and, as the tumor further expands, cells will die from the lack of supply of oxygen and nutrients. This will lead to regions of necrosis enclosed by a rim of hypoxia, as was seen in the E106 tumors. Interestingly, our results suggest that the spatial distribution of perfused vessels might act as an indirect indicator of hypoxia in gliomas in, for example, noninvasive studies, where tracers are used to detect the perfused microvessels. More evidence for this suggestion was found in a recent noninvasive MRI study by Van der Sanden *et al.* (42), showing that

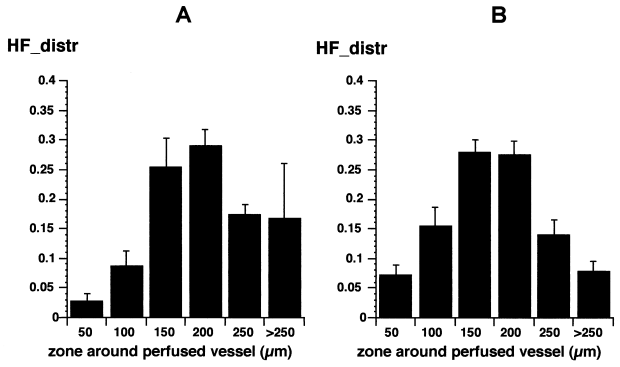

Fig. 8. Quantitative analysis of the distribution of hypoxia, visualized with either NITP (A) or pimonidazole (B) in tumor sections of a human glioma xenograft (E106), in relation to the perfused vasculature. The proportion of the total hypoxic area (HF−distr), distributed over six arbitrary zones of 50 μm, 100 μm, 150 μm, 200 μm, 250 μm, and $>$ 250 μm around perfused blood vessels, was measured. Bars represent the mean of three sections and the error bars represent the standard error of the mean.

Gadolineum−DTPA distribution was positively related to the perfused microvessel density in hypoxic 9L-gliomas growing in rat brain.

Although our results strongly suggest the existence of only diffusion-limited (chronic) hypoxia, the occurrence of perfusion-limited (acute) hypoxia in these tumors cannot be completely excluded. As temporal fluctuations in tumor blood flow have been found for a period of several minutes to hours (10, 43), and given the fact that we applied a time interval of 2 h of hypoxia marker administration, it is clear that our present method may not detect acute hypoxia in gliomas. However, recent unpublished data show that the presence of pimonidazole for a period of 20–30 min is sufficient to stain all hypoxic areas. The use of pimonidazole in addition to NITP administration in the same tumor with a certain time interval might reveal temporal changes in hypoxia, which could be regarded as acute hypoxia.

Table 2. Effect of variations in threshold settings on hypoxia parameters in one section of a NITP-stained tumor (NITP) and pimonidazole stained-tumor (PIMO) after repeated analysis of sections

change in pixel value from originally set threshold (29)	NITP		PIMO	
	HF*	HDmin†	HF*	HDmin†
−4 (−13.8%)	0.22	102	0.21	98
−2 (−6.9%)	0.17	111	0.19	105
0 (0%)	0.14	125	0.17	109
+2 (6.9%)	0.12	128	0.16	112
+4 (13.8%)	0.10	128	0.14	118
mean	0.15	119	0.17	108
CV (%)‡	31.3	9.9	15.5	6.9

* = hypoxic fraction
† = minimal distances from perfused vessels to the nearest hypoxic area
‡ = coefficient of variation

When this technique is combined with dual perfusion markers (Hoechst 33342 and DiOC) (21, 44), temporal differences in perfusion might be quantitatively studied. These dual-marker techniques are now being developed in our institute and show promising results.

In addition to measurements of minimal hypoxic distances, the proportion of all hypoxic cells distributed over arbitrary zones around (perfused) vessels (Fig. 8) can be analyzed in tumor cross-sections. Also, this parameter will reveal the development of necrosis at the far end of hypoxic regions from (perfused) vessels, as nitroimidazoles only bind to viable, hypoxic cells (45). This is because active metabolism is required to form immunological recognizable molecules (29, 34). The main advantage of this parameter is that it can be obtained rather quickly from a large number of images compared to the partially interactive measurement of minimal hypoxic distances.

Both the Hoechst signal (perfusion) and the endothelium marker exhibited a bright fluorescence signal that allowed clear segmentation from the background. Due to this thresholding operation, information about intensity differences in these signals was lost; however, this was not considered critical (22) because one of the main purposes of this study was to quantitatively assess the spatial distribution of the (perfused) vasculature. It was assumed that the distribution of the hypoxia markers NITP and pimonidazole throughout the tumors was not perfusion-limited, and was established by free diffusion of these markers from perfused vessels into the tumor tissue. Also, it was unlikely that both hypoxia markers had an adverse effect on tumor blood perfusion, because this was shown to occur only at very high doses (100–1,000 mg/kg mouse weight) (46). Assuming that there is a gradual oxygen gradient to lower values from vessels into the surrounding tissue, the rapid increase from background to maximum level of the green fluorescence hypoxia signal at a certain distance from vessels (Fig. 5) indicated that only cells with low oxygen concentrations were detected with both hypoxia markers. This is consistent with data from other studies, showing a steep rise in binding of the 2-nitroimidazole, misonidazole, at pO_2 values below 10 mmHg in multicellular spheroids (47), and comparable K_m and binding patterns of pimonidazole (35). The advantage of the existence of such a steep gradient is that it allows visually clear isolation of these hypoxic cells from the rest of the tumor within a small range of pixel values. As a consequence of this, variations in threshold values outside this range will influence the outcome of hypoxic parameters (Table 2). While this effect is most prominent for the calculation of the hypoxic fraction, the influence on the minimal hypoxic distance is less pronounced. Therefore, only one fixed threshold should be used when analyzing sections from the same study. This can be achieved by staining these sections with the same protocol in one series. When comparing measurements using different hypoxia markers, caution is needed when interpreting the results. The differences in staining between pimonidazole and NITP in our study might partially explain the higher hypoxic

Table 3. Effect of variations in threshold settings on the proportion of hypoxia distributed over six arbitrary zones in one section of a NITP-stained tumor and pimonidazole-stained tumor after repeated analysis of sections.

Marker	Change in pixel value from originally set threshold (29)	HF_distr*					
		50 (μm)	100 (μm)	150 (μm)	200 (μm)	250 (μm)	$>$ 250 (μm)
NITP	−4 (−13.8%)	0.10	0.18	0.25	0.22	0.13	0.12
NITP	−2 (−6.9%)	0.09	0.17	0.26	0.23	0.13	0.12
NITP	0 (0%)	0.09	0.17	0.26	0.24	0.14	0.11
NITP	+2 (6.9%)	0.08	0.16	0.26	0.24	0.13	0.12
NITP	+4 (13.8%)	0.08	0.15	0.26	0.24	0.14	0.12
	mean	0.09	0.17	0.26	0.23	0.13	0.12
	CV (%)†	8.9	7.1	1.6	4.5	2.6	5.5
pimo	−4 (−13.8%)	0.18	0.18	0.24	0.19	0.12	0.09
pimo	−2 (−6.9%)	0.18	0.17	0.23	0.20	0.12	0.10
pimo	0 (0%)	0.18	0.17	0.23	0.20	0.13	0.10
pimo	+2 (6.9%)	0.18	0.16	0.23	0.20	0.13	0.10
pimo	+4 (13.8%)	0.19	0.16	0.23	0.20	0.13	0.10
	mean	0.18	0.17	0.23	0.20	0.12	0.10
	CV (%)†	1.2	5.0	1.0	1.5	2.9	1.7

* = proportion of hypoxia distributed over six arbitrary zones with a width of 50 μm around perfused vessels
† = coefficient of variation

fractions and lower minimal hypoxic distances in the pimonidazole-stained tumors. As pimonidazole is found closer to the vessels (Fig. 5), the result is a shorter minimal hypoxic distance and a larger tissue area occupied by the marker (higher hypoxic fraction). Another possible explanation could relate to the charge on the pimonidazole, which cause the marker to accumulate in the acidic parts of the tumor. With NITP, a more even distribution is expected, and therefore a more diffuse staining. Another important issue is that pimonidazole is highly soluble in water and was injected i.v., while NITP was administered i.p. as a peanut oil suspension. Therefore, delivery of NITP to the tumor can be more critical than when pimonidazole is used. Moreover, pimonidazole can be given to patients (4, 5, 32, 33), allowing analyses of tumor hypoxia in clinical studies.

A number of invasive and noninvasive methods have been used for quantification of hypoxia in tumors. While nuclear medicine techniques have the advantage of being noninvasive (48), flow cytometry measurements (34, 49), polarography (50), and immunohistochemical assays (51, 52) can reveal one or more different morphological and physiological parameters with larger resolutions at microregional levels. Although these measurements do not always correlate (53, 54), the different procedures can be complementary to each other. For example, the novel fiberoptic fluorosensor (55), which measures tissue pO_2, can simultaneously be used during NMR measurements. With the image analysis system described here, relationships between hypoxia and perfused vasculature can be spatially studied in whole sections as well as in selected regional areas. Moreover, when combined with proliferation markers, it is possible to simultaneously study cell kinetics in relation to hypoxia and perfusion in histological sections (56). One of our main goals is to monitor vascular, hypoxia, and proliferation parameters as a guide for choosing the most suitable treatment strategy; however, our technique also permits quantitative analysis of changes of these parameters in response to irradiation, blood flow modifiers, and hypoxia modifiers (18, 57).

In conclusion, the multiple-staining technique described here not only allows quantitative characterization of perfusion, vasculature, and hypoxia in tumors, but it also permits quantitation of spatial relationships between these parameters in a tumor model.

REFERENCES

1. Suit HD. Hyperbaric oxygen in radiotherapy of four mouse tumors. *Proc Int Conf Radiat Biol Cancer* 1966;1:39–43.
2. Thomlinson RH. Changes of oxygenation in tumors in relation to irradiation. *Front Radiat Ther Oncol* 1968;3:109–121.
3. Moulder JE, Rockwell S. Hypoxic fractions of solid tumors: Experimental techniques, methods of analysis, and a survey of existing data. *Int J Radiat Oncol Biol Phys* 1984;10:695–712.
4. Kennedy AS, Raleigh JA, Perez GM, *et al*. Proliferation and hypoxia in human squamous cell carcinoma of the cervix: First report of combined immunohistochemical assays. *Int J Radiat Oncol Biol Phys* 1997;37:897–905.
5. Raleigh JA, Calkins-Adams DP, Rinker LH, *et al*. Hypoxia and vascular endothelial growth factor protein expression in human tumors. *Cancer Res* 1998;58:3765–3768.
6. Rockwell S, Moulder JE. Hypoxic fractions of human tumors xenografted into mice: A review. *Int J Radiat Oncol Biol Phys* 1990;19:197–202.
7. Vaupel P, Schlenger K, Knoop C, *et al*. Oxygenation of human tumors: Evaluation of tissue oxygen distribution in breast cancers by computerized O_2 tension measurements. *Cancer Res* 1991;51:3316–3322.
8. Thomlinson RH, Gray LH. The histological structure of some human lung cancers and the possible implications for radiotherapy. *Br J Cancer* 1955;9:539–549.
9. Brown JM. Evidence for acutely hypoxic cells in mouse

tumours and a possible mechanism for reoxygenation. *Br J Radiol* 1979;52:650–656.
10. Dewhirst MW, Kimura H, Rehmus SWE, *et al*. Microvascular studies on the origins of perfusion-limited hypoxia. *Br J Cancer* 1996;74(Suppl. 27):S247–S251.
11. Awwad HK, El Naggar M, Mocktar N, *et al*. Intercapillary distance measurement as an indicator of hypoxia in carcinoma of the cervix uteri. *Int J Radiat Oncol Biol Phys* 1986;12: 1329–1333.
12. Secomb TW, Hsu R, Dewhirst MW, *et al*. Analysis of oxygen transport to tumor tissue by microvascular networks. *Int J Radiat Oncol Biol Phys* 1993;25:481–489.
13. Groshar D, Mcewan AJB, Parliament MB, *et al*. Imaging tumor hypoxia and tumor perfusion. *J Nucl Med* 1993;34:885–888.
14. Goda F, Bacic G, Ohara JA, *et al*. The relationship between partial pressure of oxygen and perfusion in two murine tumors after x-ray irradiation: A combined gadopentetate dimeglumine dynamic magnetic resonance imaging and in vivo electron paramagnetic resonance oximetry study. *Cancer Res* 1996;56:3344–3349.
15. Horsman MR, Nordsmark M, Khalil AA, *et al*. Reducing acute and chronic hypoxia in tumours by combining nicotinamide with carbogen breathing. *Acta Oncol* 1994;33:371–376.
16. Olive PL. Radiation-induced reoxygenation in the SCCVII murine tumour: Evidence for a decrease in oxygen consumption and an increase in tumour perfusion. *Radiother Oncol* 1994;32:37–46.
17. Van Geel IPJ, Oppelaar H, Rijken PFJW, *et al*. Vascular perfusion and hypoxic areas in RIF-1 tumours after photodynamic therapy. *Br J Cancer* 1996;73:288–293.
18. Bussink J, Kaanders JHAM, Rijken PFJW, *et al*. Vascular architecture and microenvironmental parameters in human squamous cell carcinoma xenografts: Effects of carbogen and nicotinamide. *Radiother Oncol* 1999;50:173–184.
19. Bernsen HJ, Rijken PF, Peters JPW, *et al*. Suramin treatment of human glioma xenografts; effects on tumor vasculature and oxygenation status. *J Neurooncol* 1999;44:129–136.
20. Bernsen HJ, Rijken PF, Peters JPW, *et al*. Hypoxia in an intracerebral human glioma model. *J Neurosurg*. Submitted.
21. Fenton BM, Paoni SF, Lee J, *et al*. Quantification of tumour vasculature and hypoxia by immunohistochemical staining and HbO(2) saturation measurements. *Br J Cancer* 1999;79: 464–471.
22. Rijken PFJW, Bernsen HJJA, van der Kogel AJ. Application of an image analysis system to the quantitation of tumor perfusion and vascularity in human glioma xenografts. *Microvasc Res* 1995;50:141–153.
23. Bernsen HJJA, Rijken PFJW, Oostendorp T, *et al*. Vascularity and perfusion of human gliomas xenografted in the athymic nude mouse. *Br J Cancer* 1995;71:721–726.
24. Bernsen HJJA, Rijken PFJW, Peters JPW, *et al*. Delayed vascular changes after antiangiogenic therapy with antivascular endothelial growth factor antibodies in human glioma xenografts in nude mice. *Neurosurgery* 1998;43:570–575.
25. Bernsen HJJA, Rijken PFJW, Peters JPW, *et al*. The effect of the anti-angiogenic agent TNP-470 on tumor growth and vascularity in low passaged xenografts of human gliomas in nude mice. *J Neurooncol* 1998;38:51–57.
26. Van der Sanden BPJ, Rijken PFJW, Heerschap A, *et al*. In vivo P-31 magnetic resonance spectroscopy and morphometric analysis of the perfused vascular architecture of human glioma xenografts in nude mice. *Br J Cancer* 1997;75:1432–1438.
27. Van der Sanden BPJ, Heerschap A, Simonetti, AW, *et al*. Characterization and validation of noninvasive oxygen tension measurements in human glioma xenografts by 19F-MR relaxometry. *Int J Radiat Oncol Biol Phys* 1999;44:649–658.
28. Hodgkiss RJ, Wardman P. The measurement of hypoxia in tumours. *BJR Suppl* 1992;24:105–110.
29. Raleigh JA, Miller GG, Franko AJ, *et al*. Fluorescence immunohistochemical detection of hypoxic cells in spheroids and tumours. *Br J Cancer* 1987;56:395–400.
30. Evans, S, Joiner B, Jenkins WT, *et al*. Identification of hypoxia in cells and tissues of epigastric 9L rat glioma using EF5 [2-(2-nitro-1H-imidazol-1-yl)-N-(2,2,3,3,3-pentafluoropropyl) acetamide]. *Br J Cancer* 1995;72:875–882.
31. Laughlin K, Evans S, Jenkins WT, *et al*. Biodistribution of the nitroimidazole EF5 (2-[2-nitro-1H-imidazol-1-yl]-N-(2,2,3,3,3-pentafluoropropyl) acetamide) in mice bearing subcutaneous EMT6 tumors. *J Pharmacol Exp Ther* 1996;277:1049–1057.
32. Evans SM, Hahn S, Pook DR, *et al*. Detection of hypoxia in human squamous cell carcinoma by EF5 binding. *Cancer Res*. 2000;60:2018–2024.
33. Varia MA, Calkins-Adams DP, Rinker LH, *et al*. Pimonidazole: A novel hypoxia marker for complementary study of tumor hypoxia and cell proliferation in cervical carcinoma. *Gynecol Oncol* 1998;71:270–277.
34. Hodgkiss RJ, Jones G, Long A, *et al*. Flow cytometric evaluation of hypoxic cells in solid experimental tumours using fluorescence immunodetection. *Br J Cancer* 1991;63:119–125.
35. Arteel GE, Thurman RG, Yates JM, *et al*. Evidence that hypoxia markers detect oxygen gradients in liver: Pimonidazole and retrograde perfusion of rat liver. *Br J Cancer* 1995; 72:889–895.
36. Pötgens AJG, Lubsen NH, van Altena MC, *et al*. Vascular permeability factor expression influences tumor angiogenesis in human melanoma lines xenografted to nude mice. *Am J Pathol* 1995;146:197–209.
37. Westphal JR, van Thullenaar RGM, van der Laak JAWM, *et al*. Vascular density in melanoma xenografts correlates with vascular permeability factor expression but not with metastatic potential. *Br J Cancer* 1997;76:561–570.
38. Azuma C, Raleigh JA, Thrall, DE. Longevity of pimonidazole adducts in spontaneous canine tumors as an estimate of hypoxic cell lifetime. *Radiat Res* 1997;148:35–42.
39. Freitas I, Bono B, Bertone V, *et al*. Characterization of the metabolism of perinecrotic cells in solid tumors by enzyme histochemistry. *Anticancer Res* 1996;16:1491–1502.
40. Tannock IF. The relation between cell proliferation and the vascular system in a transplanted mouse mammary tumor. *Br J Cancer* 1969;22:258–273.
41. Vaupel P, Kallinowski F, Okunieff P. Blood flow, oxygen and nutrient supply, and metabolic microenvironment of human tumors: A review. *Cancer Res*1989;49:6449–6465.
42. Van der Sanden BPJ, Rozijn TH, Rijken PFJW, *et al*. Noninvasive assessment of the functional neovasculature in gL-glioma growing in rat brain by dynamic ^{1}H magnetic resonance imaging of gadolinium uptake. *JCBFM* 2000;20:861–870.
43. Pigott KH, Hill SA, Chaplin DJ, *et al*. Microregional fluctuations in perfusion within human tumours detected using laser Doppler flowmetry. *Radiother Oncol* 1996;40:45–50.
44. Trotter MJ, Chaplin DJ, Durand RE, *et al*. The use of fluorescent probes to identify regions of transient perfusion in murine tumors. *Int J Radiat Oncol Biol Phys* 1989;16:931–934.
45. Durand RE, Raleigh JA. Identification of nonproliferating but viable hypoxic tumor cells in vivo. *Cancer Res* 1998;58:3547–3550.
46. Chaplin DJ, Horsman MR. Tumor blood flow changes induced by chemical modifiers of radiation response. *Int J Radiat Oncol Biol Phys* 1992;22:459–462.
47. Gross MW, Karbach U, Groebe K, *et al*. Calibration of misonidazole labeling by simultaneous measurement of oxygen

tension and labeling density in multicellular spheroids. *Int J Cancer* 1995;61:567–573.
48. Chapman JD, Engelhardt EL, Stobbe CC, *et al*. Measuring hypoxia and predicting tumor radioresistance with nuclear medicine assays. *Radiother Oncol* 1998;46:229–237.
49. Webster L, Hodgkiss RJ, Wilson GD. Simultaneous triple staining for hypoxia, proliferation, and DNA content in murine tumours. *Cytometry* 1995;21:344–351.
50. Nordsmark M, Hoyer M, Keller J, *et al*. The relationship between tumor oxygenation and cell proliferation in human soft tissue sarcomas. *Int J Radiat Oncol Biol Phys* 1996;35: 701–708.
51. Cline JM, Thrall DE, Rosner GL, *et al*. Distribution of the hypoxia marker CCI-103F in canine tumors. *Int J Radiat Oncol Biol Phys* 1994;28:921–933.
52. Raleigh JA, Zeman EM, Calkins DP, *et al*. Distribution of hypoxia and proliferation associated markers in spontaneous canine tumors. *Acta Oncol* 1995;34:345–349.
53. Kavanagh MC, Sun A, Hu QY, *et al*. Comparing techniques of measuring tumor hypoxia in different murine tumors: Eppendorf pO(2) histograph, [H-3]misonidazole binding and paired survival assay. *Radiat Res* 1996;145:491–500.
54. Nozue M, Lee I, Yuan F, *et al*. Interlaboratory variation in oxygen tension measurement by Eppendorf "histograph" and comparison with hypoxic marker. *J Surg Oncol* 1997; 66:30–38.
55. Young WK, Vojnovic B, Wardman P. Measurement of oxygen tension in tumours by time-resolved fluorescence. *Br J Cancer* 1996;74:S256–S259.
56. Bussink J, Kaanders JHAM, Rijken PFJW, *et al*. Multiparameter analysis of vasculature, perfusion and proliferation in human tumour xenografts. *Br J Cancer* 1998;77:57–64.
57. Bussink J, Kaanders JHAM, Rijken PFJW, *et al*. Changes in blood perfusion and hypoxia after irradiation of a human squamous cell carcinoma xenograft tumor line. *Radiat Res* 2000;153:398–404.